Morphology of High Impact Polypropylene Particles†

Idoia Urdampilleta, Alba González, Juan J. Iruin, José C. de la Cal, and José M. Asua*

Institute for Polymer Materials (POLYMAT), The University of the Basque Country, Apdo 1072, 20018 Donostia-San Sebastián, Spain

Received December 16, 2004; Revised Manuscript Received January 13, 2005

ABSTRACT: An extensive characterization (SEM, AFM, mercury porosimetry, sorption, and ^{13}C NMR) of the particle morphology prior (isotactic PP particles) and after the gas phase reaction (hiPP particles) was performed in an attempt to gain some knowledge of the gas phase reaction of the hiPP process. It was found that the majority of the elastomer was finely dispersed in the i-PP matrix, but breaking the i-PP matrix and flowing into its pores. It was also found that the interior of the particles was readily accessible to the monomers because of the existence of a network of pores. The catalyst fragmented into small pieces with about ≈210 atoms of Ti per fragment. The copolymer is richer in ethylene than in propylene although the monomer concentration around the active center is $[C_3]/[C_2] = 2.75$. This behavior could not be justified on the basis of a faster diffusivity of the ethylene with respect to the propylene and hence must be due to higher activity of the catalyst for ethylene.

Introduction

High impact polypropylene (hiPP) is a high-tech commodity polymer widely used in injection molding parts for automotive. With a yearly increase of 10%, hiPP is one of the fastest growing polymers. hiPP is a complex material formed by a matrix of isotactic polypropylene in which a poly(ethylene−propylene) elastomeric copolymer (EPR) is finely dispersed. hiPP is a "product-by-process" produced in two stages in series. First, isotactic PP particles are produced in liquid propylene using a Ziegler−Natta catalyst. These particles are transferred to a gas phase fluidized reactor where the elastomeric phase is produced within the isotactic polypropylene. hiPP properties mainly depend on particle morphology, which is determined by the processes occurring in the second reactor. Although the process is a commercial success, its understanding is far from perfect, largely due to the lack of a thorough characterization of the resulting product.

Only a limited number of studies on hiPP morphology have been published,[1−4] and because of the complexity of the problem, any model satisfied completely the growth and morphology of these particles.

The mechanism of polymer growth described by Debling[1] and by Debling and Ray[2] is largely based on the double grain structure proposed by Kakugo et al.[5,6] for the polypropylene particles formed in the homopolymerization stage. According to this model, the polypropylene particle is formed by quite a few mesoparticles (called polymer globules by Kakugo et al.[6]) of relatively small size (≈1 μm). Each mesoparticle is formed by primary polymer particles containing a catalyst crystallite. Such structure contains macropores separating the mesoparticles and micropores that separates the microparticles. The EPR formed in the second stage does not remain encapsulated within the polypropylene microparticles but progressively expands into the small micropores and then into larger macropores. McKenna et al.[4] proposed that the EPR which is formed on the active sites located on the surface of the catalyst crystallites underneath the layer of PP homopolymer creates stresses in the viscoelastic PP homopolymer, leading to the formation of cracks in the PP. The EPR will then flow through the cracks, into the micro- and macropores, and onto the surface of the polymer particle.

Cecchin et al.[3] proposed that at the end of the homopolymerization stage the polypropylene particle is composed by quite a few polymer mesoparticles. According to these authors, the catalyst fragments are located at the surface of the polymer mesoparticles because they segregated during the homopolymerization. Therefore, the EPR formed in the second stage is located at the surface of these mesoparticles filling the pores between them. This leads to a continuous network of EPR.

The goal of this work is to gain knowledge of the second stage through an extensive analysis of the particle morphology prior (isotactic PP particles) and after the gas phase reaction (hiPP particles). Key aspects of the particle morphology include the following: (i) The *porous structure of the particles*, which is critical for the accessibility of the monomers to the active centers. (ii) The *distribution of the elastomer within the isotactic PP matrix*, which determines the properties of the material and affects the runability of the process because if the elastomer reaches the surface of the particles, they become sticky and the fluidized bed may clog. In addition, the distribution of the elastomer is a measure of the fragmentation of the catalyst and its distribution through the particle. (iii) The *type of copolymer produced*, which provides information about the activity distribution of the active centers as well as the relative accessibility of the monomers (ethylene and propylene) to them.

Experimental Section

Commercial samples of isotactic PP and hiPP from a Spheripol process (Basell) were supplied by Repsol-YPF. The isotactic PP particles were produced in the first reactor and constitute the feed of the fluidized bed reactor. The hiPP

† This article is dedicated to Prof. Cecilia Sarasola.

* To whom correspondence should be addressed: e-mail jmasua@sq.ehu.es.

10.1021/ma047413v CCC: $30.25
Published on Web 02/19/2005

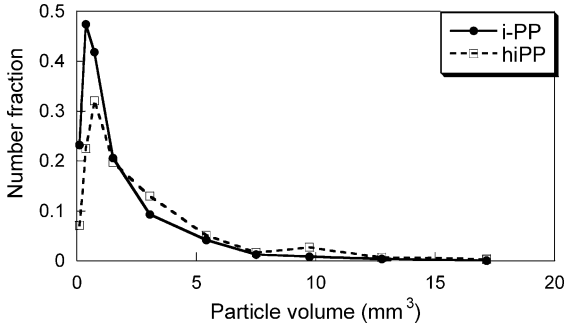

Figure 1. Particle size distribution of the i-PP and hiPP.

particles were the product of this second reactor. The average rubber content of the hiPP particles was 24 wt % as determined by ^{13}C NMR. The samples are particulate with the particle size distributions given in Figure 1. The particles were characterized as follows:

Rubber Extraction. EPR was extracted by placing the particles in a Soxhlet for 7 days in boiling *n*-hexane.

Scanning Electron Microscopy (SEM). The whole particles as well as cryosectionated particles were coated with gold and then examined in the SEM.

Atomic Force Microscopy (AFM). To prepare the samples for AFM analysis, the particle was first cut in such a way that a small rectangular prism protruded from the rest of the surface (see illustration in Figure 7). The surface of the prism should not be bigger than 100 μm × 100 μm, preferentially smaller.[7] Larger surfaces make much more difficult the subsequent cryoultramicrotomy. The surface for AFM analysis was prepared by cryoultramicrotomy[8] of the protruding prim using a Leica ultracut UCT ultramicrotome. A cutting speed of 0.05 mm/s and a temperature of −80 °C were used.

The AFM measurements were performed with a Nanoscope IV from Digital Instruments. All scans were performed with commercial Si Nanoprobes SPM tips. Height, phase, and amplitude images were performed simultaneously in tapping mode at the fundamental resonance frequency of the Si cantilever with typical scan rates of 0.5 line/s. The free oscillating amplitude was 2.0 V, while the set point amplitude was individually chosen for each sample.

Mercury Intrusion Porosimetry. The pore structure was determined by mercury intrusion in an Autopore II 9220.

Sorption Measurements. Gravimetric sorption experiments were carried out in an electromagnetic balance IGA 2 (Hiden). It operates with gases and vapors in a wide range of temperatures and up to 20 bar. It can be programmed in both sorption and desorption experiments, where the pressure is increased or decreased in a step by step mode. The experimental results of the gained mass of propylene or ethylene in particles or in a film at a determinate pressure and temperature were modeled using the solution of the material balances for these geometries[9] (eqs 1 and 3, respectively).

$$\frac{M_t - M_0}{M_\infty - M_0} = 1 - \frac{6}{\pi^2}\sum_{n=1}^{\infty}\frac{1}{n^2}\exp(-Kn^2t) \quad (1)$$

where

$$K = \frac{D_{\text{eff}}\pi^2}{r^2} \quad (2)$$

$$\frac{M_t - M_0}{M_\infty - M_0} = 1 - \frac{8}{\pi^2}\sum_{n=0}^{\infty}\frac{1}{(2n+1)^2}\exp(-K(2n+1)^2t) \quad (3)$$

where

$$K = \frac{D_{\text{eff}}\pi^2}{l^2} \quad (4)$$

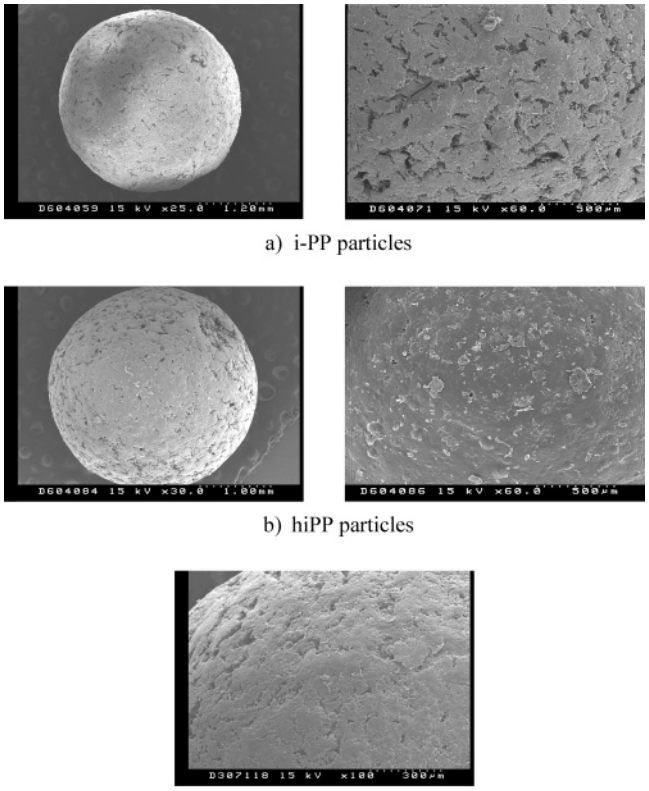

a) i-PP particles

b) hiPP particles

c) hiPP particles after extraction with boiling hexane

Figure 2. Comparison between the external surfaces of i-PP and hiPP.

In these equations, M_0 is the initial mass of either the film or the particles, M_t and M_∞ are the mass of the samples at time t (seconds) and under equilibrium, r and l are the effective diffusion length in the particles and in the film, respectively, and D_{eff} is the effective diffusion coefficient.

Results and Discussion

Figure 2 compares the external surface of the hiPP particles (Figure 2b) with that of the i-PP particles (Figure 2a) as observed by SEM. It can be seen that the particles are very spherical in shape, showing that the original shape of the homopolymer particle (and presumably that of the catalyst) was retained during the copolymerization stage. However, the texture of their surfaces differed. The surface of the particles became smoother upon copolymerization of ethylene−propylene, suggesting that the elastomer filled some of the pores of the precursor i-PP particles. At higher magnifications the nature of the particle surface is more clearly illustrated. This suggests that the elastomeric phase filled in the pores of the particles. This is further supported by the fact that the surface of the hiPP particles becomes rougher (similar to that of the i-PP) upon dissolving the elastomer with boiling hexane (Figure 2c).

In an attempt to obtain a direct observation of the internal porous structure of the particles, i-PP and hiPP particles were cut into two pieces by using a cryoultramicrotome. One of the pieces was directly coated with gold and observed by SEM. Figure 3 presents the SEM pictures of the cross section of i-PP (Figure 3a) and hiPP (Figure 3b). It can be seen that the i-PP particles showed larges pores, whereas the hiPP particles did not show apparent pores. A closer look to the cross section of the hiPP particles shows that the surface

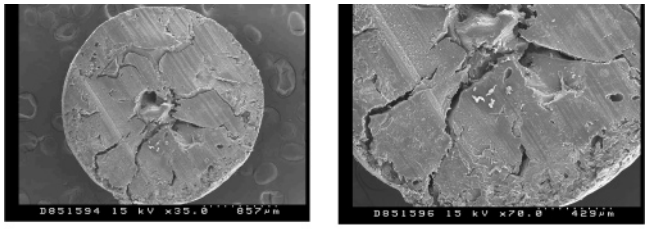

a) Cross-section of i-PP particles

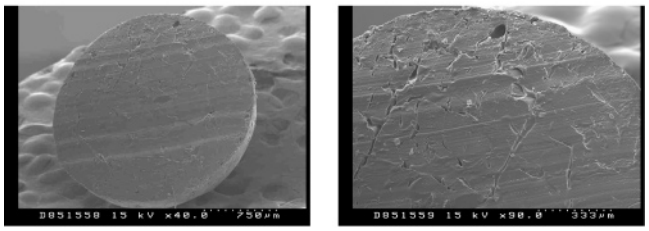

b) Cross-section of hiPP particles

Figure 3. SEM pictures of cross sections of i-PP and hiPP particles.

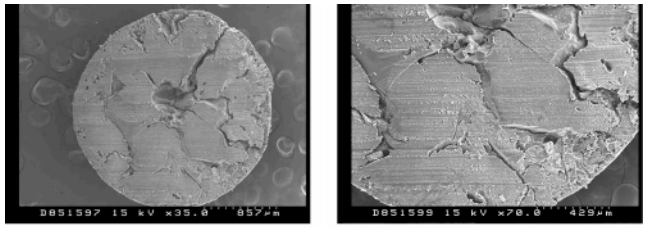

a) Cross-sections of i-PP particles extracted with boiling hexane

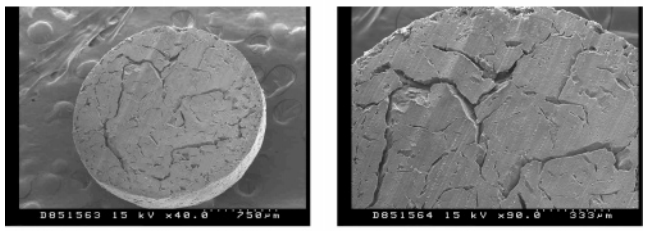

b) Cross-sections of hiPP particles extracted with boiling hexane

Figure 4. SEM pictures of cross sections of i-PP and hiPP particles after extraction with boiling hexane.

is not regular, although this irregularity may be due to the cut with the cryoultramicrotome. In any case, the results in Figure 3 further support the idea that the ethylene−propylene copolymer fills the pores of the i-PP particles.

The other half of the particle was extracted with boiling hexane for 7 days. Then, it was coated with gold and observed by SEM. Figure 4 presents the SEM micrographs of the cross sections of the particles after extraction with hexane. Comparison with Figure 3 shows that the internal structure of the i-PP particles was not affected by the extraction. On the other hand, a porous structure similar to that of the i-PP appeared in the hiPP when the elastomer was dissolved with boiling hexane. This strongly indicates that the elastomer produced in the second reactor filled the pores of the i-PP particles. However, it could be argued that this is an artifact caused by the blade of the ultramicrotome that could spread the elastomer onto the polypropylene surface (in a way similar to spreading butter on a toast). Thermal damage occurring during sputtering may also contribute to the smoothing of the surface, but it is unlikely that this was the reason for the apparent

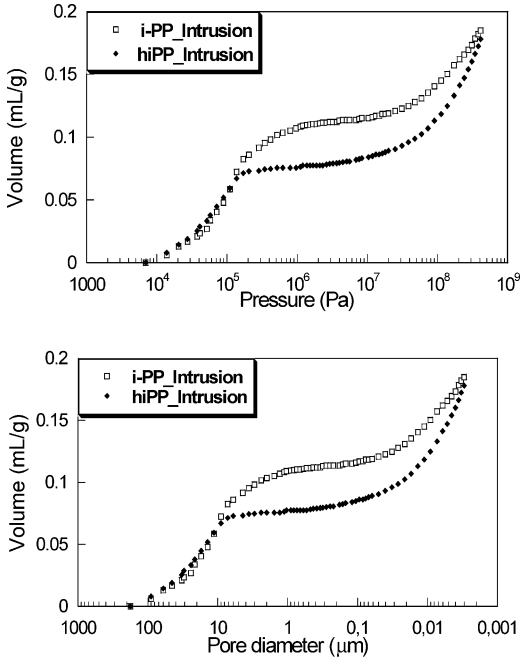

Figure 5. Mercury porosimetry data for i-PP and hiPP particles.

absence of pores. To clarify this point, the porous structure of these particles was characterized by both mercury porosimetry and by measuring the apparent diffusion coefficients.

Figure 5 presents the mercury porosimetry data for i-PP and hiPP particles. This figure shows two distinct increases of the volume as the pressure increased. The first one corresponds to pores in the range of 10−50 μm, which coincides remarkably well with the pore sizes observed in the SEM micrographs. The apparent pore volume at pressures over 7×10^7 Pa was due to the compressibility of the material. Figure 5 also shows that the overall porosity of the i-PP particles (about 12%) was substantially higher than that of the hiPP particles (about 7%), indicating that only about 46% of the pores were filled with the elastomer. This also indicates that the absence of pores in the SEM picture of the cross section of hiPP (Figure 3b) might be due to an artifact of the microtomization process. This point is further discussed below.

Information about the porous structure may also be obtained from the sorption experiments. In these experiments, the weight increase of the polymer particles in contact with a gas (ethylene or propylene) at a given pressure is monitorized. These experiments allow the calculation of an apparent mass transfer rate coefficient, K, which is related to the effective diffusion coefficient, D_{eff}.

In a particle such as that presented in Figure 3a, the sorption involves two processes in series: first, the diffusion of the ethylene (or propylene) through the pores, and second, the diffusion through the amorphous fraction of the solid polymer. This second process is the slower one and therefore the rate-controlling step. Consequently, in the case of the particle in Figure 3a, r (see eq 2) is the size of the solids fragments that are among pores. On the other hand, Figure 3b suggests that the characteristic size of the hiPP should be close to the radius of the whole particle. Therefore, the estimation of r gives an indication of the porosity of the particle.

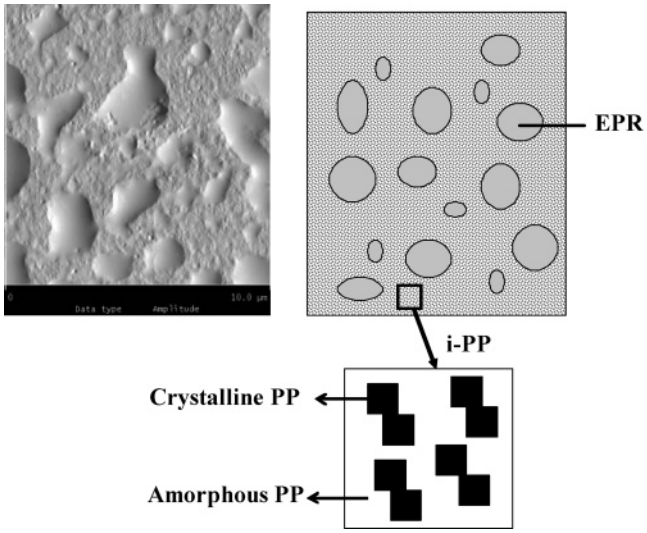

Figure 6. Diffusion model.

To estimate r from eq 2, a value for D_{eff} should be estimated from independent measurements. Figure 6 presents an AFM picture of a hiPP particle. It can be seen that the elastomer (zones with smooth surface) is distributed inside the i-PP matrix. The effective diffusion rate coefficient for such a system is given by the following equation:

$$\frac{1}{D_{\text{eff\_hiPP}}} = \frac{\epsilon_e}{D_e} + \frac{1-\epsilon_e}{D_{\text{eff\_iPP}}} \tag{5}$$

where $D_{\text{eff\_hiPP}}$ and $D_{\text{eff\_i–PP}}$ are the effective diffusion rate coefficient in the hiPP particles and in the i-PP matrix, ϵ_e is the volume fraction of elastomer, and D_e is the diffusion rate coefficient of the monomer in the elastomer.

The volume fraction of the elastomer ($\epsilon_e = 0.34$) was determined from the overall composition measured by ^{13}C NMR. The diffusion coefficient of propylene in the elastomer was experimentally measured from sorption experiments on an EPR film (formed using the ethylene−propylene copolymer extracted from the particles) of known thickness ($l = 295\ \mu$m) at 60 °C and 1, 3, 5, and 7 bar of pressure. The fitting of these experiments with eqs 3 and 4 allowed the estimation of the diffusion coefficient of propylene in EPR, $D_e = 8.1 \times 10^{-7}$ cm^2/s.

Therefore, the only unknown parameter in eq 5 is $D_{\text{eff\_i–PP}}$. The i-PP matrix is composed by crystalline and amorphous polypropylene, and the monomer may only diffuse through the amorphous phase. $D_{\text{eff\_i–PP}}$ is estimated applying the random pore model.[10,11] This model represents the crystalline parts by the squares in Figure 6, and the spaces between them represent the amorphous phase. In addition, the model assumes that the area void fractions are the same as the volume void fractions.

As the monomer cannot diffuse through the crystalline phase, the only available way is through the amorphous phase:

$$D_{\text{eff\_}i\text{ – PP}} = \epsilon_{a1}{}^2 D_a \tag{6}$$

where ϵ_{a1} is the volume fraction of the amorphous phase referred to the i-PP matrix and D_a is the diffusion coefficient in the amorphous phase. ϵ_{a1} is calculated based on ϵ_a (volume fraction of the amorphous phase referred to the overall particle).

$$\epsilon_{a1} = \frac{\epsilon_a}{1-\epsilon_e} = \frac{\epsilon_a}{\epsilon_a + \epsilon_c} \tag{7}$$

where the volume fraction of the crystalline phase referred to the overall particle (ϵ_c) was determined by DSC experiments of the hiPP particles.

To calculate the D_a, the effective diffusion coefficient of propylene in a i-PP film was measured at 60 °C and at different pressures (1, 3, 5, and 7 bar), and the random pore model was applied. The values of ϵ_c and ϵ_a for the film were determined by DSC ($\epsilon_c = 0.48$, $\epsilon_a = 0.52$). The diffusion coefficient of propylene in the amorphous phase was $D_a = 5.32 \times 10^{-7}$ cm^2/s.

Once all the parameters were known, the values of r for i-PP and hiPP particles were determined. They are given in Table 1. It can be seen that the characteristic length for hiPP was greater than that of i-PP but still substantially smaller than the particle size. This means that in agreement with the porosimetry measurements and contrary to what was suggested by Figure 3b, the hiPP particles retained a significant porosity. On the other hand, for both i-PP and hiPP particles, the size of the mesoparticles was substantially larger than that proposed by Kakugo et al.[5] Table 1 also includes the estimated number of mesoparticles per particle, N_p.

Table 2 shows the same parameters as in Table 1 but corresponding to experiments done with ethylene ($D_e = 1.31 \times 10^{-6}$ cm^2/s and $D_a = 8.90 \times 10^{-7}$ cm^2/s). It can be observed that the results of both tables agreed very well.

Table 1. Estimated Values of the Characteristic Length for Diffusion for Propylene in i-PP and hiPP Particles at 60 °C

	K (s^{-1})	ϵ_a	ϵ_e	D_{eff} (cm^2/s)	r (cm)	N_p
i-PP	2.4×10^{-3}	0.67	0	2.39×10^{-7}	3.1×10^{-2}	102
hiPP	1.35×10^{-3}	0.44	0.34	3.14×10^{-7}	4.8×10^{-2}	27

Table 2. Estimated Values of the Characteristic Length for Diffusion for Ethylene in i-PP and hiPP Particles at 60 °C

	K (s^{-1})	ϵ_a	ϵ_e	D_{eff} (cm^2/s)	r_p (cm)	N_p
i-PP	4.22×10^{-3}	0.67	0	3.99×10^{-7}	3.0×10^{-2}	113
hiPP	2.38×10^{-3}	0.44	0.34	5.23×10^{-7}	4.6×10^{-2}	31

The results presented above show that a fraction of the copolymer that is produced in the second stage filled the pores of the initial i-PP particle. From a mechanistic point of view, this may suggest that a large part of the elastomer is produced at or near the surface of the big pores, which would imply either the accumulation of catalyst near the pores or the existence of severe mass transfer limitations in the solid polymer, which cannot be justified using the measured diffusion coefficients. Another possibility is that EPR formed within the polypropylene matrix flows to the pores.

The distribution of the elastomer in the hiPP particles was determined by AFM. Three different positions were chosen: one near the surface of the particle ($r_1 \approx r_P$), another at $r_1 \approx r_P/2$, and the third one near the center of the particle ($r_1 \approx 0$). The study was performed on one hiPP particle following the procedure outlined in Figure 7. First, the particle was microtomized near the surface (level 1) and observed in the AFM. After observation, the same particle was microtomized to level 2, and after the AFM measurement, the procedure was repeated for level 3.

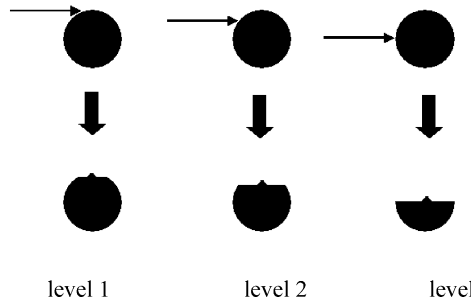

Figure 7. Radial positions at which the distribution of the elastomer was examined by AFM.

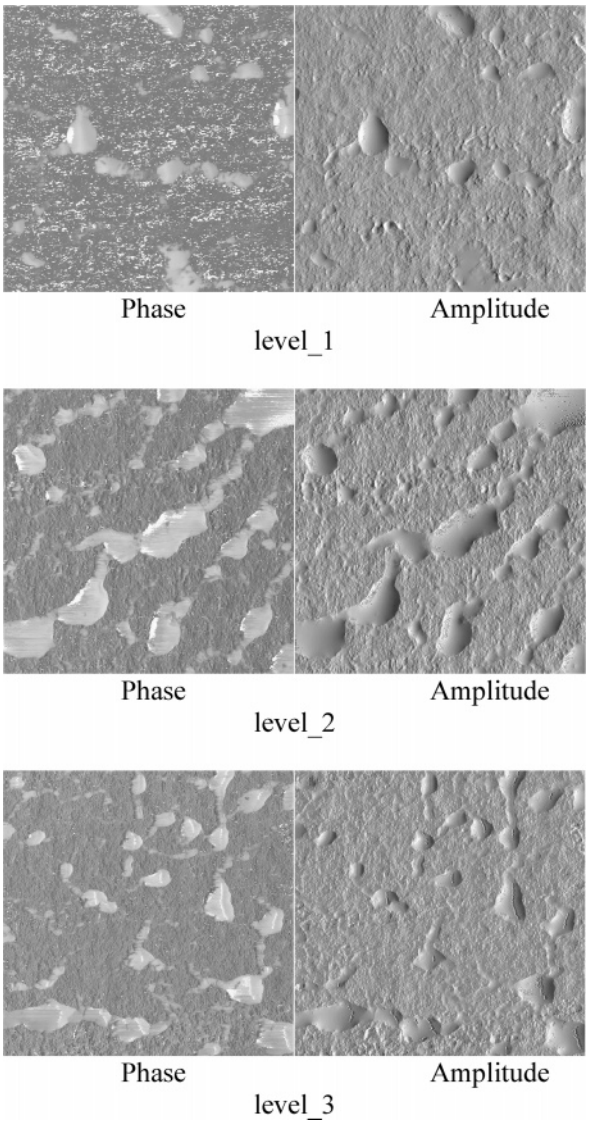

Figure 8. Phase and amplitude images of hiPP particle at three different levels of deep. Scan size 10 μm.

Figure 8 presents the phase contrast images obtained along the particle radius. It can be observed that the elastomer was finely distributed within the polypropylene matrix, appearing as isolated rubbery domains. This is in conflict with the model for hiPP particle growth proposed by Debling et al.[2] It also challenges the model proposed by Cecchin et al.,[3] in which the catalyst fragments are located at the surface of the polymer subglobules. Actually, the combination of AFM, porosimetry, and sorption results suggests a morphology of the polymer particle different from what was proposed by previous authors. This point will be discussed below.

Table 3. Percentage of Copolymer Area and Average Copolymer Inclusion Area at Different Radial Positions in the hiPP Particle

	EPR area (%)	inclusion average area (μm^2)
P_n1	6.1	0.4
P_n2	19.5	1.0
P_n3	14.7	0.6

On the other hand, it seems that there was less elastomer near the surface of the particle than in levels 2 and 3. This may indicate that the catalyst concentration near the surface of the particle was lower than within the particle or that the elastomer produced near the surface migrated to the surface, filling the irregularities of the particle surface (see Figure 2). It may be argued that this may be an artifact as the cut was performed very close to the surface of the particle, but quite a few particles were examined, and this result was found in all the cases. The average values of the surface covered by the elastomer and the average size of one inclusion are given in Table 3. These data can be used to estimate the fraction of EPR that is dispersed within the i-PP matrix.

The volume fraction of EPR in the i-PP matrix was 17.1% (considering a homogeneous material), namely about 72% of the total EPR. This means that about 28% of the EPR is in the pores and fills approximately 56% of the pores, which agrees reasonably well with the estimation from mercury porosimetry.

Data in Table 3 also allow estimating the number of EPR inclusions in the i-PP matrix, which can be taken as a rough estimation of the number of catalyst fragments.

$$\text{number of inclusions} = \frac{\frac{4}{3}\pi R^3}{\frac{4}{3}\pi r_i^3}(1-\epsilon_p)F \qquad (8)$$

where R is the radius of the whole particle, ϵ_p is the porosity of the i-PP, r_i is the actual ratio of the inclusion, and F is the fraction of elastomer in the matrix. Assuming that the inclusions were spheres, a random cut of the spheres yields circles with an average cross-sectional area which is smaller than the cross-section area at the equator of the particles. Geometric considerations allow to estimate the ratio between the apparent to the actual ratio as

$$\frac{r_i}{r_{app}} = \sqrt{\frac{3}{2}} \qquad (9)$$

where r_{app} is the apparent radius of the inclusion, which can be estimated from the average inclusion area (Table 3).

For a particle of 2.5−2.8 mm in diameter, eq 8 predicts about 1×10^9 fragments of catalyst. The titanium content was measured using atomic absorption spectroscopy, giving 0.25 μg of Ti/g of polymer. This means that as an average each fragment contained approximately 210 atoms of Ti.

Figure 8 also shows some indications of connectivity between elastomeric domains, suggesting that the elastomer produced on the surface of the catalyst fragments breaks the i-PP matrix flowing through the cracks created. Likely, the cracks would be oriented toward the

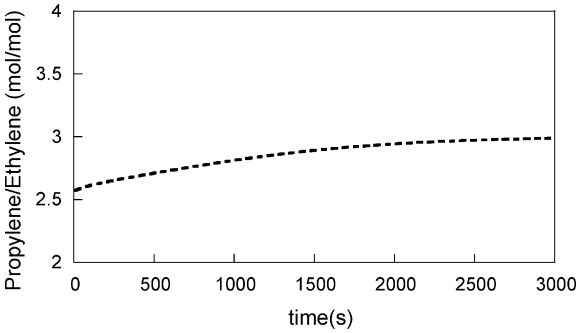

Figure 9. Estimated evolution of the average monomer molar ratio in the hiPP particle.

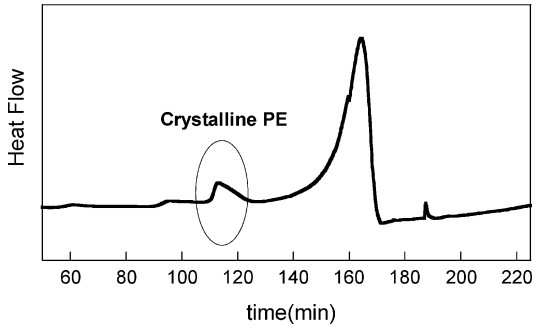

Figure 10. DSC of hiPP particles.

Table 4. Copolymer Composition Based on ^{13}C NMR Diads

	diads			molar composition	
extract	%PP	%EP	%EE	%P	%E
hiPP	16.3	47.6	36.1	40.1	59.9

weakest part of the material, i.e., toward the pores, and hence a significant part of the EPR (about 28%) ended filling the pores. It is open to discussion whether catalyst fragments encapsulated in the EPR were transported to the pores by the flowing EPR. Once at the surface of the pores, they would be more accessible to the monomers, leading to a faster rate of EPR formation. The results presented here also challenge the model proposed by McKenna et al.[4] in which the pores are formed by catalyst coated by polypropylene, and upon copolymerization of ethylene/propylene on the catalyst, the EPR formed breaks the polypropylene coating filling the pores.

The type of copolymer produced was analyzed in an attempt to obtaining information about the reactivity of the monomers as well as the relative accessibility of the monomers (ethylene and propylene) to the active centers. The copolymer was separated from the i-PP by extraction. Five grams of particles was extracted in a Soxhlet for 7 days with boiling hexane. The extract was analyzed by ^{13}C NMR, and the results are given in Tables 4 and 5. Table 4 shows the molar composition based on diads, and Table 5 shows the molar composition based on triads. These tables show that the copolymer was richer in ethylene than in propylene.

To clarify if this effect was due to diffusional limitations or to intrinsic reactivity ratios, sorption experiments using propylene and ethylene were carried out with hiPP particles. From these data, the diffusion coefficients for ethylene and propylene were determined. This allowed the calculation of the evolution of the average propylene/ethylene molar ratio in the polymer particles during a simulated sorption experiment. Figure 9 shows that the propylene/ethylene monomer ratio slightly increased over time, having an average value higher than one, $C_3/C_2 = 2.75$, even through ethylene diffused faster than propylene ($K_{ethylene} = 2.1 \times 10^{-3}\ s^{-1}$; $K_{propylene} = 1.50 \times 10^{-3}\ s^{-1}$). This was due to the higher sorption of the propylene.

In a copolymerization which follows the terminal model, the diads and triads are given by

$$PP = y_P P_{PP} \tag{10}$$

$$EP = y_P P_{PE} + y_E P_{EP} \tag{11}$$

$$EE = y_E P_{EE} \tag{12}$$

$$PPP = y_P P_{PP}^2 \tag{13}$$

$$PPE = y_P P_{PP} P_{PE} + y_E P_{EP} P_{PP} \tag{14}$$

$$PEP = y_P P_{PE} P_{EP} \tag{15}$$

$$EPE = y_E P_{EP} P_{PE} \tag{16}$$

$$EEP = y_P P_{PE} P_{EE} + y_E P_{EE} P_{EP} \tag{17}$$

$$EEE = y_E P_{EE}^2 \tag{18}$$

where y_P and y_E are the copolymer compositions referred to propylene and ethylene, respectively.

$$y_P = \frac{1 + r_P X}{r_P X + \frac{r_E}{X} + 2} \tag{19}$$

$$y_E = 1 - y_P \tag{20}$$

and

$$P_{PP} = \frac{r_P X}{1 + r_P X} \tag{21}$$

$$P_{EE} = \frac{r_E}{r_E + X} \tag{22}$$

where X is the average propylene/ethylene molar ratio

$$P_{PE} = 1 - P_{PP} \tag{23}$$

$$P_{EP} = 1 - P_{EE} \tag{24}$$

in the polymer particles. The reactivity ratios were estimated using eqs 10−24 to fit the experimental data in Tables 4 and 5. The values obtained were $r_E = 4.4$ and $r_P = 0.38$. Therefore, the relative enrichment of the copolymer in ethylene was due to a higher reactivity ratio.

The average length of the propylene and ethylene sequences can be calculated as follows:

$$\overline{l_P} = 1 + r_P X \tag{25}$$

$$\overline{l_E} = 1 + \frac{r_E}{X} \tag{26}$$

The average length of the propylene sequence was 2.04 and that of the ethylene 2.60. This value for the

Table 5. Copolymer Composition Based on ^{13}C NMR Triads

	triads						molar composition	
extract	%PPP	%PPE	%EPE	%PEP	%EEP	%EEE	%P	%E
hiPP	11.9	21.2	11.0	8.9	23.9	23.1	43.6	56.4

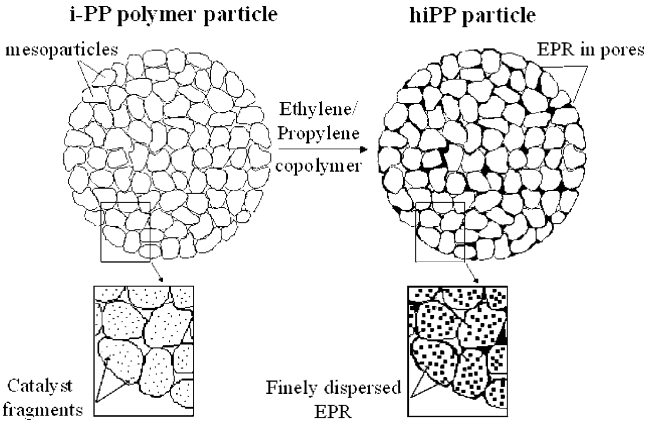

Figure 11. Model for hiPP particle growth.

ethylene is somehow surprising because DSC data show the presence of crystalline polyethylene (Figure 10). This suggests the presence of the active centers which preferentially polymerize ethylene. The NMR data were reevaluated using the approach proposed by Cheng,[12] assuming that the catalyst contained two active centers. The best fit the dual-site catalyst was

$$\text{center 1: } f = 44.6\%;\ r_E = 1.89;\ r_P = 0.51$$

$$\text{center 2: } f = 55.6\%;\ r_E = 7.32;\ r_P = 0.25$$

where f is the fraction of each type of center. The average length of the ethylene sequence for center 2 calculated with eq 26 is 3.66, which still seems to be short for the formation of crystalline domains of polyethylene.

Conclusions

The results presented in this paper show that the i-PP particles are formed by a relatively small number (about 100) of mesoparticles. The average size of the mesoparticles is about one-fifth of the particle diameter. In each mesoparticle, the catalyst fragments (about 10^7 per mesoparticle) are well dispersed within the polypropylene matrix (Figure 11). No proof of a finer morphology was obtained. All mesoparticles are equally reachable for the monomers as the diffusion through the pores between mesoparticles is not rate limiting. This means that the propylene polymerization could be modeled by means of the polymeric flow model applied to each mesoparticle.

The copolymerization of ethylene and propylene in the second stage fluidized bed leads to the formation of EPR around the catalyst fragments, yielding a composite morphology of finely dispersed EPR in the polypropylene matrix. Most of the EPR is within this composite mesoparticles. Some of the elastomer (about 28%) breaks the polypropylene matrix and flows to the pores reducing the porosity of the whole particle. A part of this elastomer finds its way to the surface of the polymer particle smoothing the surface. It is a matter of speculation whether catalyst fragments encapsulated by the elastomer are brought to the surface of the mesoparticles (to the pores) by the flowing EPR, and once there they contribute to the formation of EPR in the pores.

^{13}C NMR analysis of the EPR showed that ethylene was preferentially incorporated into the copolymer. This was not due to a faster diffusivity of the ethylene but to a higher reactivity ratio for the ethylene ($r_E = 4.4$; $r_P = 0.38$). These reactivity ratios and the average monomer molar ratio in the mesoparticles estimated from sorption experiments could not justify the presence of crystalline polyethylene detected in the DSC experiments, which strongly suggests the existence of ethylene specific active centers.

Acknowledgment. The financial support form the European Commission (project POLYPROP, No. GRD2-2000-30189) and the supply of samples by Repsol-YPF are acknowledged.

References and Notes

(1) Debling, J. A. Modeling particle growth and morphology of impact polypropylene produced in the gas phase. Ph.D. Thesis, University of Wisconsin, 1997.
(2) Debling, J. A.; Ray, W. H. *J. Appl. Polym. Sci.* **2001**, *81*, 3085−3106.
(3) Cecchin, G.; Marchetti, E.; Baruzzi, G. *Macromol. Chem. Phys.* **2001**, *202*, 1987−1994.
(4) Mckenna, T.; Bouzid, D.; Matsunami, S.; Sugano, T. *Polymer React. Eng.* **2003.** *11*, 177−197.
(5) Kakugo, M.; Sadatoshi, H.; Yokoyama, M.; Kojima, K. *Macromolecules* **1989**, *22*, 551−557.
(6) Kakugo, M.; Sadatoshi, H.; Sakai, J.; Yokoyama, M. *Macromolecules* **1989**, *22*, 3172−3177.
(7) Tanem B. S.; Kamfjord, T.; Augestad, M.; Lovgren, T. B.; Lundquist, M. *Polymer* **2003**, *44*, 4283−4291.
(8) Gedde, U. W. *Polymer Physics*; Chapman & Hall: London, 1995.
(9) Crank, J. *The Mathematics of Diffusion*; Clarendon Press: Oxford, 1975.
(10) Wakao, N.; Smith, J. M. *Chem. Eng. Sci.* **1962**, *17*, 825−834.
(11) Wakao, N.; Smith, J. M. *Ind. Eng. Chem. Fundam.* **1964**, *3*, 123−127.
(12) Cheng, H. N. In *Computer Applications in Applied Polymer Science II;* Provder, T., Ed.; *ACS Symp. Ser.* **1989**, *404*, 174−188.

MA047413V